Pore structure model for elastic wave velocities in fluid-saturated sandstones

E. C. David[1] and R. W. Zimmerman[1]

Received 1 February 2012; revised 31 May 2012; accepted 2 June 2012; published 21 July 2012.

[1] During hydrostatic compression conducted within the elastic regime, P and S-wave velocities measured on porous rock samples generally increase with pressure and reach asymptotic values at high pressures. The increase in velocities can be attributed to the gradual closure of compliant cracks, in which case the high-pressure velocities reflect only the influence of the stiff, non-closable pores. A procedure is presented to extract the complete pore aspect ratio distribution from the pressure dependence of dry velocities, assuming that the rock contains a distribution of cracks with different aspect ratios, and one family of stiff pores having an aspect ratio that generally will lie between 0.01 and 1. The model is able to invert successfully many sets of experimental data on dry sandstones taken from the literature. The pore aspect ratio distribution inverted from dry data can then be used to predict saturated velocities as functions of pressure, by introducing fluid into the pores. For ultrasonic velocity measurements that are performed at high frequencies in the laboratory ($\sim$ MHz), the predictions of saturated velocities using effective medium theories match well the experimental data for a good number of sandstone data sets. The saturated velocities thus predicted are always more accurate than those predicted from the Gassmann relations, which underpredict the saturated velocities by a large amount. These results are only weakly dependent on the choice of the effective medium theory.

Citation: David, E. C., and R. W. Zimmerman (2012), Pore structure model for elastic wave velocities in fluid-saturated sandstones, *J. Geophys. Res.*, *117*, B07210, doi:10.1029/2012JB009195.

1. Introduction

[2] Elastic properties of porous rocks depend on mineralogical composition, porosity, and pore fluid properties, but are also greatly dependent on pore structure. A large number of theoretical works have been dedicated to relating the so-called "effective elastic properties" to the microstructure. Due to the complexity of the pore space in rocks, these works contain two levels of approximation. The first one idealizes the shape of the pores, generally by assuming that they can be represented by spheroids characterized by their aspect ratio α. These spheroidal pores can represent a wide variety of pore shapes, and are amenable to analytical treatment through the formalism of *Eshelby* [1957]. The second level of approximation involves the way interactions (of stress and strain fields) between pores are accounted for. Effective medium theories provide a tool to extend Eshelby's results to non-dilute concentrations of pores.

[3] Elastic velocities have been measured in sandstones for decades [*King*, 2005], notably by the travel-time method in the laboratory using P and S-wave transducers glued onto the sample, under independently controlled confining and pore fluid pressures. During hydrostatic compression, V_p and V_s increase with pressure, and reach asymptotic values at high pressures, provided that the rock remains in the elastic regime. The increase of elastic velocities with pressure is attributed to crack closure: when the confining pressure increases, "compliant" thin cracks successively close up at pressures that are proportional to their aspect ratios [*Walsh*, 1965]; hence, the value attained by the high-pressure velocities must only reflect the influence of the "stiff", non-closable pores.

[4] Consequently, the pressure dependence of velocities can be inverted to obtain the pore aspect ratio distribution. *Morlier* [1971] devised a method to extract the aspect ratio distribution directly from the dry rock compressibility (either measured by static methods, or calculated from elastic velocities). This method ignores stress field interactions between nearby cracks, and so is accurate only for rocks containing low crack densities. *Zimmerman* [1991] extended Morlier's method by using an effective medium theory to account for the nonlinear variation of compressibility with crack density. Zimmerman's method can be used in conjunction with any effective medium theory. However, this method is not able to extract the aspect ratios of the stiff, non-closable pores. *Cheng and Toksöz* [1979] performed a joint inversion of dry and saturated velocities on various

[1]Department of Earth Sciences and Engineering, Imperial College London, London, UK.

Corresponding author: E. C. David, Department of Earth Sciences and Engineering, Imperial College London, London SW7 2AZ, UK. (emmanuel.david08@imperial.ac.uk)

0148-0227/12/2012JB009195

sandstones, assuming a discrete distribution of aspect ratios. However, their method is only valid for the Kuster-Toksöz effective medium scheme [*Kuster and Toksöz*, 1974]. They used a crack closure law that was not consistent with their equation for the bulk compressibility, and their method only yields an aspect ratio distribution that is defined at a finite number of aspect ratios. *Agersborg et al.* [2008] inverted aspect ratio distributions from dry data on carbonates, which were then used to predict saturated velocities that were compared to the predictions of the Gassmann relations. However, their analysis is complex and involves a very large number of fitting parameters. *Fortin et al.* [2007] and *Adelinet et al.* [2011] inverted (separately) dry and saturated velocities on a Vosges sandstone and an Icelandic basalt, respectively. Their analysis is simple, but they assume that the non-closable pores are spherical, which is not realistic; they also assume that cracks have only one "average" aspect ratio that is inverted at each pressure, without using a crack closure equation to relate aspect ratio to the pressure, which would be necessary in order to obtain the initial crack aspect ratio distribution at zero pressure.

[5] One way to accurately account for the non-linear elastic behavior of porous rocks during hydrostatic compression is to assume that the rock contains a distribution of aspect ratios. Although dry velocities do not depend on the crack aspect ratios, but only on the crack density at a given pressure, the pressure dependence of dry velocities does indeed allow for inversion of the crack aspect ratio distribution, by considering the crack closure process. The first aim of this paper, in section 2, is therefore to invert the pressure dependence of dry velocities to obtain the complete aspect ratio distribution, extending Zimmerman's method. It is assumed that the rock contains a distribution of crack aspect ratios, along with one family of stiff pores having an aspect ratio lying somewhere between 0.01 and 1. The model is developed in two versions, using the Mori-Tanaka effective medium scheme [*Mori and Tanaka*, 1973; *Benveniste*, 1987; *Ferrari*, 1994], which allows simple analytical treatment, and the Differential effective medium scheme [*Salganik*, 1973; *McLaughlin*, 1977; *Zimmerman*, 1984; *Norris*, 1985], which is very robust even at high pore concentrations. The inversion is done using data obtained in dry experiments (after *Fortin et al.* [2007] and *David* [2012]), since pore fluids have a strong effect on velocities, and tend to mask the effects of pore geometry. This new method is also much simpler to implement than a complicated joint inversion of dry and saturated data, such as that performed by *Cheng and Toksöz* [1979].

[6] It would be very useful to develop a pore structure model that is able to *predict* the (fully) saturated velocities, for any fluid present in the pores, noting that at a given differential stress, the pore structure should be the same as during a dry test. *Gassmann* [1951] proposed equations that expressed the undrained elastic moduli as functions of drained moduli (which, according to poroelasticity theory, are equal to dry moduli [*Bourbié et al.*, 1986]), without any assumption regarding the microstructure. However, Gassmann assumed that there is local equilibrium of fluid pressure within the pore space, which is not necessarily the case for ultrasonic measurements that are performed at high frequencies (~ MHz). The high-frequency behavior might be better described by the use of effective medium theories, which implicitly assume that the fluid is trapped in each individual pore. Hence, in section 3, fluid is introduced into the aspect ratio distribution function obtained from dry data, to test the predictions of effective medium theories against two experimental data sets on sandstones.

2. Inversion of Dry Seismic Velocities

2.1. Method for Obtaining the Pore Aspect Ratio Distribution

[7] Consider an isotropic rock core loaded under dry and quasi-static conditions at various hydrostatic pressures, in the elastic regime, and that the following measurements are available: P and S-wave velocities, (V_p, V_s), as functions of increasing hydrostatic pressure, p; the rock density, ρ; the mineralogical composition, from which the effective elastic moduli of the mineral phase can be inferred using the Voigt-Reuss-Hill average; and the porosity, ϕ.

[8] Recall that the elastic bulk and shear moduli (K, G) can be directly calculated from the wave velocities:

$$K = \rho\left(V_p^2 - \frac{4}{3}V_s^2\right), \tag{1}$$

$$G = \rho V_s^2. \tag{2}$$

[9] Effective medium theories provide a very useful tool to relate elastic properties to the microstructure. The effective elastic moduli of an elastic medium containing dry pores can be expressed as function of the porosity, the pore geometry, and the elastic moduli of the minerals. According to the Mori-Tanaka scheme, the effective moduli (K,G) of an isotropic solid containing one family of randomly oriented pores, having one aspect ratio, are described by the following equations [*Benveniste*, 1987]:

$$\frac{K_0}{K} = 1 + \frac{\phi}{1-\phi}P, \tag{3}$$

$$\frac{G_0}{G} = 1 + \frac{\phi}{1-\phi}Q, \tag{4}$$

where ϕ is the porosity, (K_0, G_0) are the bulk and shear moduli of the mineral phase, and (P, Q) are, respectively, the normalized pore compressibility and shear compliance of the pores. For spheroids, exact analytical expressions for P and Q are available, but due their length are not reproduced here; they can be found in *David and Zimmerman* [2011a]. For dry pores, the pore compliances are functions only of the spheroid aspect ratio, α, and the solid Poisson's ratio, ν_0, where $\nu_0 = (3K_0 - 2G_0)/6K_0 + 2G_0)$. According to the Differential scheme, the effective moduli (K,G) are governed by a pair of coupled differential equations [*LeRavalec and Guéguen*, 1996]:

$$(1-\phi)\frac{1}{K}\frac{dK}{d\phi} = -P, \tag{5}$$

$$(1-\phi)\frac{1}{G}\frac{dG}{d\phi} = -Q, \tag{6}$$

with the initial conditions $K(\phi = 0) = K_0$ and $G(\phi = 0) = G_0$.

2.1.1. High-Pressure Data and Stiff Porosity

[10] A value for the aspect ratio of the stiff pores can be extracted from the high-pressure data, assuming that all cracks are then closed. This can be considered to be a realistic assumption if measurements of V_p and V_s are available at a pressure sufficiently high so that the velocities reach asymptotic values. If this is not the case, they can still be obtained assuming that the bulk compressibility $C_{bc} = 1/K$ and shear compliance $S = 1/G$, decay exponentially with confining pressure p; as far as the compressibility is concerned, this empirical law has been shown to represent well the behavior of many sandstones [*Zimmerman*, 1991]:

$$C_{bc} = (C_{bc}^{i} - C_{bc}^{hp})e^{-p/\hat{p}} + C_{bc}^{hp}, \tag{7}$$

$$S = (S^{i} - S^{hp})e^{-p/\hat{p}} + S^{hp}, \tag{8}$$

where the superscript "i" refers to initial values (at zero pressure), "hp" refers to high-pressure values, and $\hat{p}$ is a scaling factor, with dimensions of pressure, that characterizes the rate at which the compliances level off. Such fits, actually for the moduli rather than the compliances, have recently been tested successfully against many sets of experimental data on sandstones by *MacBeth* [2004]. Theoretical justifications of expressions (7) and (8) have been proposed by *Shapiro* [2003] and *Liu et al.* [2009].

[11] The first step in the method is to invert the high-pressure velocities (V_p^{hp}, V_s^{hp}) to obtain the best value of the aspect ratio of the non-closable pores, α^{hp}, which is assumed to lie between 0.01 (a slightly inflated oblate spheroidal crack) and 1 (a spherical pore). The choice of the aspect ratio range is not arbitrary: the closure pressure of a pore is roughly equal to αE_0 (in the no-interaction approximation), where E_0 is the solid-phase Young's modulus [*Walsh*, 1965]; hence, the closure of a pore having an aspect ratio $\alpha = 0.01$, in a typical sandstone ($E_0 \sim 50$ GPa), would require a pressure equal to 500 MPa, which is far beyond the value that would cause inelastic pore collapse. It is therefore not necessary to consider values of α lower than 0.01 when inverting the aspect ratio of the non-closable pores.

[12] The ensuing effective medium modeling considers that the family of stiff pores is embedded in the mineralogical matrix with elastic moduli (K_0, G_0), and that the total porosity ϕ is matched by such pores. The parameter α^{hp} is inverted independently for the Mori-Tanaka scheme and the Differential scheme, by a least squares regression of high-pressure velocity data. The inversion procedure minimizes the error on V_p^{hp} and V_s^{hp} (with equal weights), forcing the total porosity to be matched. The forward modeling solutions are obtained by converting the elastic moduli, which are given by the sets of equations (3)–(4) and (5)–(6) for the Mori-Tanaka scheme and the Differential scheme, respectively, into velocities, remembering that α^{hp} is contained in the expressions for (P, Q). Note that, for the Differential scheme, solutions of the differential equations (in the forward modeling sense) are obtained using a Runge-Kutta algorithm. Indeed, although some approximate analytical solutions can be found for a wide range of aspect ratios ($\alpha < 0.3$), they do not cover the entire range $0.01 < \alpha^{hp} < 1$ [*David and Zimmerman*, 2011b].

[13] The values of high-pressure moduli, which are obtained from the inversion, are referred to as ($K^{hp,mt}$, $G^{hp,mt}$) and ($K^{hp,dem}$, $G^{hp,dem}$) for the Mori-Tanaka scheme and the Differential scheme, respectively. The purpose of this notation is to avoid confusion with (K^{hp}, G^{hp}), which are the experimentally measured values.

[14] A key point to remember is that the presence of non-closable pores does not introduce any pressure dependence into the elastic moduli (see notably the analysis proposed by *Shapiro* [2003]). The aspect ratio of a stiff pore changes very slightly with pressure, but as long as these pores remain open, they contribute an additional term in the bulk compliance that is independent of pressure. The pressure dependence is caused only by the presence of cracks that successively close up. Hence, it can be considered that, at each pressure, such cracks are simply introduced into a host material formed by the minerals plus the stiff pores.

2.1.2. Inversion of Crack Densities

[15] In the case of penny-shaped dry cracks, with aspect ratios lower than 0.01, P and Q are inversely proportional to α [*David and Zimmerman*, 2011a]. Inserting these expressions into the sets of equations (3)–(4) and (5)–(6) leads to simple expressions for the effective moduli [*David and Zimmerman*, 2011b]. They are functions of the crack density parameter Γ [*Walsh*, 1965], which is defined as

$$\Gamma = \frac{N\langle a^3 \rangle}{V}, \tag{9}$$

where N is the number of circular cracks (of radius a) in a representative elementary volume V, and the angle brackets symbolize an average. The crack density is then related to the total crack porosity ϕ_c by

$$\phi_c = \frac{4}{3}\pi\alpha\Gamma. \tag{10}$$

[16] For the Mori-Tanaka scheme, the expressions giving the effective moduli (K,G) reduce to the no-interaction approximation, because as cracks represent a very small volume fraction, the term $(1 - \phi)$ in the denominator on the right-hand side of equations (3) and (4) becomes negligible. Hence, for cracks,

$$\frac{K^{hp,mt}}{K} = 1 + \frac{16\left[1 - \left(\nu^{hp,mt}\right)^2\right]\Gamma}{9(1 - 2\nu^{hp,mt})}, \tag{11}$$

$$\frac{G^{hp,mt}}{G} = 1 + \frac{32\left(1 - \nu^{hp,mt}\right)\left(5 - \nu^{hp,mt}\right)\Gamma}{45(2 - \nu^{hp,mt})}, \tag{12}$$

where ($K^{hp,mt}$, $G^{hp,mt}$) are the bulk and shear moduli of the host material composed of the minerals and the non-closable pores, and are found from the inversion of the high-pressure data using the Mori-Tanaka scheme, and where $\nu^{hp,mt} = (3K^{hp,mt} - 2G^{hp,mt})/(6K^{hp,mt} + 2G^{hp,mt})$.

[17] According to the Differential scheme, K and ν can be expressed as explicit functions of Γ [*David and Zimmerman*, 2011b], as follows:

$$\frac{K}{K^{hp,dem}} = \frac{\left(1 - 2\nu^{hp,dem}\right)e^{-16\Gamma/9}}{1 - 2\nu^{hp,dem}e^{-8\Gamma/5}}, \tag{13}$$

$$\frac{\nu}{\nu^{hp,dem}} = e^{-8\Gamma/5}, \tag{14}$$

where, now, ($K^{hp,dem}$, $G^{hp,dem}$) are the bulk and shear moduli of the host material composed of the minerals and the non-closable pores, which are found from the inversion of high-pressure data using the Differential scheme, and where $\nu^{hp,dem} = (3K^{hp,dem} - 2G^{hp,dem})/(6K^{hp,dem} + 2G^{hp,dem})$.

[18] The expressions relating the effective moduli to the crack density, for both the Mori-Tanaka and the Differential schemes, do not depend on the value of the crack aspect ratio, α, as long as α remains lower than 0.01. At each pressure p, the value of $\Gamma(p)$ can be inverted by a least squares regression on the measured velocities V_p and V_s. The values $\Gamma(p)$ decrease with p, since cracks successively close up. The next step to obtain the crack aspect ratio distribution function $\Gamma(\alpha)$ is to consider the change of crack aspect ratios with pressure. At this stage, it is worth presenting the derivation steps of Zimmerman's method [*Zimmerman*, 1991] in the next section. The steps followed in the present approach that differ from Zimmerman's method are then described in section 2.1.4.

2.1.3. Zimmerman's Method for Obtaining the Crack Aspect Ratio Distribution

[19] All the equations given in the present section are presented by *Zimmerman* [1991], except equations (18), (20) and (21), for which Zimmerman's analysis is pushed further.

[20] *Relating aspect ratio and pressure.* Consider an individual crack of aspect ratio $\alpha(p)$ at a given pressure p. The initial value of the crack aspect ratio at zero pressure is denoted by α^i, *i.e.*, $\alpha^i = \alpha(p = 0)$. The drained pore compressibility C_{pc}, which is equivalent to the dry compressibility, relates the volumetric deformation of a crack, ϵ_p, to an increment of hydrostatic pressure dp, as follows:

$$d\epsilon_p = -C_{pc}(p, \alpha^i)dp, \tag{15}$$

adopting the convention that compressive stresses or strains are positive. The volumetric deformation of a crack can be related to the change of aspect ratio, remembering that for a three-dimensional crack of length a and aperture c, *i.e.*, of aspect ratio $\alpha = c/a$, the length of the crack a can be assumed to remain unchanged during closure [*Zimmerman*, 1991]. In other words, $d\epsilon_p = d\alpha/\alpha^i$, so equation (15) can be re-written as follows:

$$d\alpha = -\left[\alpha^i C_{pc}(p, \alpha^i)\right]dp. \tag{16}$$

Hence, the aspect ratio of an individual crack can be related to the hydrostatic pressure simply by integrating the pore compressibility as a function of pressure. In doing this, a crucial step is to realize that the product αC_{pc} depends only on p but not on α. Indeed, the compressibility of a thin crack is inversely proportional to its initial aspect ratio:

$$C_{pc} = \frac{4(1-\nu^2)}{3K\pi(1-2\nu)\alpha^i}. \tag{17}$$

Although the evaluation of the elastic parameters of the "matrix" (K, ν), which are, *a priori*, functions of p, will depend on the choice of an effective medium theory, it is clear from equation (17) that αC_{pc} will remain independent of α. Integrating relation (16) between $p = 0$ and p gives

$$\alpha(p) = \alpha^i - \int_0^p \left[\alpha^i C_{pc}(p', \alpha^i)\right]dp'. \tag{18}$$

In the particular case in which p corresponds exactly to the closure pressure of a crack of initial aspect ratio α^i, $\alpha(p) = 0$ so that:

$$\alpha^i = \int_0^p \left[\alpha^i C_{pc}(p', \alpha^i)\right]dp'. \tag{19}$$

Now, at each pressure p and for any open crack ($\alpha(p) > 0$) equation (18) leads to a general form for the evolution of aspect ratio with pressure:

$$\alpha(p) = \alpha^i - \alpha^\star(p), \tag{20}$$

where, combining equations (17) and (18),

$$\alpha^\star = \int_0^p \left[\frac{4(1-\nu^2)}{3K\pi(1-2\nu)}\right]dp'. \tag{21}$$

From equation (19), $\alpha^\star(p)$ can be identified as the *minimum* value of the *initial aspect ratio* of those cracks that are still open at a given pressure p. In other words, all cracks that are open at a pressure p are cracks having initial aspect ratios $\alpha^i > \alpha^\star(p)$. Moreover, $\alpha^\star$ also represents the decrease of aspect ratio with pressure; this decrease is *independent* of the aspect ratio of the crack considered (equation (21)). Hence, in a rock containing open cracks, all crack aspect ratios decrease by the same amount between two pressure stages. Equation (20) also shows that crack aspect ratios are not necessarily linear functions of pressure, as from equation (17) the elastic moduli evaluated in the integral (21) are, in general, functions of p.

[21] *Obtaining the aspect ratio distribution.* Equation (19) provides a general relation between the initial aspect ratio of a crack and the pressure required to close that crack. The additional relation obtained between p and Γ by the use of effective medium theories (see section 2.1.2) suggests that one could obtain the crack aspect ratio distribution by changing variables from p to the crack density Γ in the integral of equation (19). However, the pore compressibility C_{pc} in equation (19) is the pore compressibility of an individual pore, whereas Γ is related to the compressibility of the entire pore space. Therefore, it is necessary to express the pore compressibility C_{pc} of the entire body in terms of the pore compressibility of individual pores. This derivation has been given in *Zimmerman* [1991], and leads to:

$$\phi_c^i C_{pc}(p) = \frac{4\pi}{3}\left[\alpha^i C_{pc}(p, \alpha^i)\right]\Gamma(\alpha^i), \tag{22}$$

where ϕ_c^i is the *initial* crack porosity (*i.e.*, at zero pressure), which should not be confused with the total porosity of the rock; and where $\Gamma(\alpha^i)$ is the cumulative aspect ratio distribution function for the crack density. $\Gamma(\alpha^i)$ represents the total crack density associated with cracks having initial aspect ratios greater than α^i, which are then still open at pressure p. Since the minimal initial aspect ratio of the open cracks at pressure p is a monotonically increasing function of p (the cracks with larger initial aspect ratios will close at higher pressures), and Γ is obviously a decreasing function of p, the aspect ratio distribution of the cumulative crack density $\Gamma(\alpha^i)$ will therefore also be a monotonically decreasing function of α^i. This suggests that Γ can be used instead of p as the variable of integration in equation (19).

Combining with the relation (22) and changing variables leads to

$$\alpha^{\mathrm{i}} = \frac{3\phi_{\mathrm{c}}^{\mathrm{i}}}{4\pi} \int_{\Gamma^{\mathrm{i}}}^{\Gamma(\alpha)} \frac{C_{\mathrm{pc}}(\Gamma)}{\Gamma} \frac{\mathrm{d}p}{\mathrm{d}\Gamma} d\Gamma, \tag{23}$$

where Γ^{i} is the initial crack density at zero pressure.

[22] The use of the bulk compressibility C_{bc} rather than C_{pc} in the integral may be more appropriate, since C_{bc} is directly measured by the seismic velocities (see equation (7)). These two compressibilities are related as follows:

$$\phi_{\mathrm{c}}^{\mathrm{i}} C_{\mathrm{pc}} = C_{\mathrm{bc}} - C_{\mathrm{bc}}^{\mathrm{hp}}, \tag{24}$$

where, according to previous considerations, $C_{\mathrm{bc}}^{\mathrm{hp}}$ is the compressibility of the host material formed by the minerals and the non-closable pores, which is independent of pressure. Inserting the relation (24) into equation (23) gives

$$\alpha^{\mathrm{i}} = \frac{3}{4\pi} \int_{\Gamma^{\mathrm{i}}}^{\Gamma(\alpha)} \frac{\left[C_{\mathrm{bc}}(\Gamma) - C_{\mathrm{bc}}^{\mathrm{hp}}\right]}{\Gamma} \frac{\mathrm{d}p}{\mathrm{d}\Gamma} d\Gamma, \tag{25}$$

where $C_{\mathrm{bc}}(\Gamma)$ is explicitly given by some effective medium theory (see equations (11) and (13) for the Mori-Tanaka and Differential schemes, respectively). Since C_{bc} is a monotonically decreasing function of Γ regardless of the effective medium theory considered, equation (25) can be rewritten (using the chain rule) in the form given by *Zimmerman* [1991]:

$$\alpha^{\mathrm{i}} = \frac{3}{4\pi} \int_{\Gamma^{\mathrm{i}}}^{\Gamma(\alpha)} \frac{\left[C_{\mathrm{bc}}(\Gamma) - C_{\mathrm{bc}}^{\mathrm{hp}}\right] \frac{\mathrm{d}C_{\mathrm{bc}}}{\mathrm{d}\Gamma}}{\frac{\mathrm{d}C_{\mathrm{bc}}}{\mathrm{d}p} \Gamma} d\Gamma, \tag{26}$$

which has the advantage of being explicitly independent of the choice of effective medium theory. The initial value of the crack density, Γ^{i}, comes from the inversion of the compressibility $C_{\mathrm{bc}}(p = 0) = C_{\mathrm{bc}}^{\mathrm{i}}$, using the $C_{\mathrm{bc}}(\Gamma)$ relation. Note that, when considering the effective medium equations for the Mori-Tanaka scheme (which, for cracks, are equivalent to the no-interaction approximation), the relation (26) can be shown to reduce to Morlier's expression [*Morlier*, 1971], as would be expected.

2.1.4. Modifications of Zimmerman's Method in the Present Approach

[23] In Zimmerman's method, which inverts the compressibility data only, $C_{\mathrm{bc}}(p)$ results from an exponential curve fit (equation (7)) and, therefore, does not depend on the choice of the effective medium theory. This approach is not followed in the present method, where it is proposed to use directly equation (25) to compute the aspect ratio distribution, instead of equation (26). The value of Γ is inverted at each pressure for the data points by minimizing the error on V_{p} and V_{s}, as was described in section 2.1.2. As there is no explicit relation between p and Γ, the evolution of crack density with pressure is assumed to obey an exponential decay law:

$$\Gamma(p) = \Gamma^{\mathrm{i}} e^{-p/\hat{p}}. \tag{27}$$

One of the advantages of such a fit, the parameters of which will depend on the effective medium theory considered, is that is gives an estimation of the initial crack density at zero pressure, whereas measurements of velocities at zero pressure are not always available. As in Zimmerman's method, the calculation of the aspect ratio distribution function comes from the integration of an analytical function, which is simple. The use of an empirical relation of the form given by equation (27) seems reasonable: for the Mori-Tanaka scheme, it is easy to see (from equation (11)) that a relation between pressure and crack density such as in equation (27), corresponds to an exponential dependence the bulk compressibility of the form (7). This is not precisely true for the Differential scheme, however, but the use of the relation (27) gives very good fits (see section 2.2).

[24] Finally, whereas in Zimmerman's method, the value $C_{\mathrm{bc}}^{\mathrm{hp}}$ is simply taken at high pressure or, alternatively, results from the exponential curve fit (equation (7)), in the present model $C_{\mathrm{bc}}^{\mathrm{hp}}$ results from the inversion of high-pressure data and will depend on the choice of effective medium theory ($C_{\mathrm{bc}}^{\mathrm{hp}} = C_{\mathrm{bc}}^{\mathrm{hp,mt}}$) or ($C_{\mathrm{bc}}^{\mathrm{hp}} = C_{\mathrm{bc}}^{\mathrm{hp,dem}}$). Zimmerman's method is thus extended here in inverting the aspect ratio of the stiff pores.

2.1.5. Computation of Related Pore Aspect Ratio Distribution Functions

[25] $\Gamma(\alpha)$ is the aspect ratio distribution of the cumulative crack density, which, as noted above, is a decreasing function of α. The aspect ratio distribution of the crack density, $\gamma(\alpha)$, can be defined as $\gamma(\alpha) = -\mathrm{d}\Gamma/\mathrm{d}\alpha$ [*Zimmerman*, 1991]. Using the relation between crack density and crack porosity given by equation (10), a crack porosity distribution function, $c(\alpha)$, can similarly be defined:

$$c(\alpha) = \frac{4\pi\alpha}{3}\gamma(\alpha), \tag{28}$$

as well as a cumulative crack porosity, $C(\alpha)$:

$$c(\alpha) = \frac{\mathrm{d}C}{\mathrm{d}\alpha}. \tag{29}$$

The aspect ratio distribution function of the cumulative crack porosity, $C(\alpha)$, should reach asymptotically a value which is simply the initial crack porosity, $\phi_{\mathrm{c}}^{\mathrm{i}}$. It can also be verified *a posteriori* that $\phi_{\mathrm{c}}^{\mathrm{i}}$ is indeed very small compared to the value of the total porosity, ϕ, validating the initial assumption that the total porosity is essentially due to the non-closable pores.

2.2. Application of Model to Experimental Data on Sandstones

[26] Measurements of ultrasonic velocities on two isotropic sandstones were obtained in the laboratory at various increasing confining pressures, under dry conditions. The measurements of *Fortin et al.* [2007] on Vosges sandstone were obtained by the commonly used "travel-time method", using P and S-wave transducers glued onto the sample. Ultrasonic measurements of (V_{p}, V_{s}) were measured at a frequency of 1 MHz, up to a confining pressure of 110 MPa (for details, see *Fortin et al.* [2007]). Measurements on Fontainebleau sandstone [*David*, 2012] were recently obtained using the same experimental setup and method as in *Fortin et al.* [2007], up to 90 MPa. Physical properties and compositions for the two samples are summarized in Table 1.

Table 1. Physical Properties and Composition of Rocks in the Present Study

Sandstone	Porosity	Bulk Density (Dry) (kg/m^3)	Mineralogical Composition
Vosges (Bleurswiller)[a]	0.235[c]	1950	50% quartz, 30% feldspars, 20% micas
Fontainebleau[b]	0.04[d]	2544	100% quartz

[a]Data after *Fortin et al.* [2007].
[b]Data after *David* [2012].
[c]The initial porosity is about 0.25; 0.235 is the estimated value of the porosity at high pressure (110 MPa) using the pore volume change (e.g., gas for dry experiments). Although the porosity change during elastic compression of the pore space is generally small (about 1.5% for this test), using the high-pressure value, instead of the zero pressure value, is more accurate for extracting the aspect ratio of the stiff pores.
[d]Zero pressure value.

[27] As explained in section 2.1.1, the first step is to invert the high-pressure velocities to estimate the aspect ratio of the stiff pores, α^{hp}. For both sets of data, as the velocities clearly reach asymptotic values, it was not necessary to use an exponential curve fit of the compressibility and shear compliance data (equations (7)–(8)) to estimate the high-pressure velocities; rather, it was assumed that the high-pressure velocities corresponded to the values measured at 110 and 90 MPa for the Vosges and Fontainebleau sandstones, respectively. For the Vosges sandstone, as the calculated Voigt-Reuss bounds for the effective moduli of the mineral phase are far apart, the high-pressure data were inverted with the elastic moduli of the grains (K_0, G_0) treated as open parameters (lying within the bounds). As far as Fontainebleau sandstone is concerned, the elastic moduli of quartz are well-documented in the literature (see Table 2). The results of the inversion, which are summarized in Table 2, show that the high-pressure elastic wave velocities of both sandstones can be well inverted assuming that the rock contains only one family of spheroidal pores, with less than 0.5% error, for either choice of the effective medium theory. This was not guaranteed, since it is clear from looking at micrographs such as in *Bourbié et al.* [1986] that real pores in sandstones do not exactly resemble spheroids. The values of α^{hp} shown in Table 2 are slightly higher for the Differential scheme than for the Mori-Tanaka scheme. Such a result is to be expected, since for the same amount of pores, the Differential scheme always predicts a more compliant behavior than does the Mori-Tanaka scheme [*David and Zimmerman*, 2011b]. Hence, if the Mori-Tanaka scheme leads to "flatter" pores, which are always more compliant [*David and Zimmerman*, 2011a], the "balance" is re-established.

[28] The cumulative crack density at each pressure is then found, as explained in section 2.1.2, by a simple least squares method minimizing the error on V_p and V_s. As expected, the estimates for the crack density are much higher for the Mori-Tanaka scheme than for the Differential scheme, since, for thin cracks, the Mori-Tanaka scheme is equivalent to the no-interaction approximation.

[29] The results of the effective medium modeling for compressional and shear velocities are represented in Figures 1 and 2 and Figures 3 and 4 for the Vosges and Fontainebleau sandstones, respectively. The results obtained

Table 2. Inversion Results for the High-Pressure Velocities (Present Model)

Sandstone	α^{hp} (MT)	Error on (V_p^{hp}, V_s^{hp}) (MT)	α^{hp} (DEM)	Error on (V_p^{hp}, V_s^{hp}) (DEM)
Vosges	0.13[a]	0.2%	0.20[a]	0.3%
Fontainebleau	0.60[b]	0.1%	0.69[b]	0.1%

[a]With K_0 = 39 GPa, G_0 = 24 GPa, that are *inverted* values for both Mori-Tanaka (MT) and Differential scheme (DEM). It was assumed that (K_0,G_0) lie within the Voigt-Reuss bounds of mineralogical components, that were calculated using the mineral properties given in *Mavko et al.* [2009].
[b]Taking K_0 = 37 GPa, G_0 = 44 GPa, for quartz [*Mavko et al.*, 2009].

by Zimmerman's method, for which inverted values of the crack density and aspect ratio of the stiff pores are fit to the compressibility data only, using the form given by equation (7), are also shown. The fitting parameters $(C_{bc}^{i}, C_{bc}^{hp}, \hat{p})$ used in Zimmerman's method are presented in Table 3, and the results for the aspect ratio of the stiff pores (inverting, then, only C_{bc}^{hp}), are presented in Table 4.

[30] This new pore structure model is more accurate in inverting the pressure dependence of elastic properties than is Zimmerman's method, although the latter has the advantage of being simpler, and gives reasonably good fits. In particular, the behavior of Poisson's ratio, which is very sensitive to the microstructure [*David and Zimmerman*, 2011b], is very well matched at all pressures by the new method (see Figures 13 and 18, where inversion of dry velocities and predictions for saturated velocities, respectively for Vosges and Fontainebleau sandstones, are summarized). This validates the use of the spheroidal model for the pores, as equally good fits have been obtained for many data sets [*David*, 2012].

[31] For both schemes, the pressure dependence of the crack density is fit reasonably well by the exponential curve fit (equation (27)). For the Vosges sandstone, according to the Mori-Tanaka scheme, $\Gamma(p) = 0.753e^{-p/9.3}$ (p in MPa)

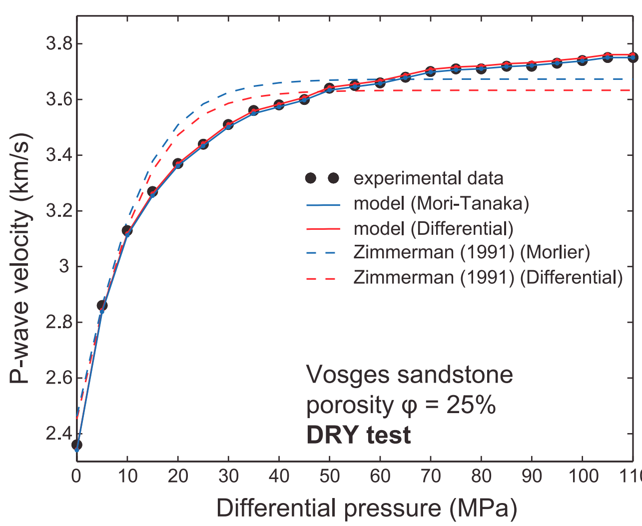

Figure 1. Inversion of V_p, compressional seismic velocity, for a dry Vosges sandstone (data after *Fortin et al.* [2007]). The present model is compared to *Zimmerman* [1991] for the Mori-Tanaka and Differential schemes.

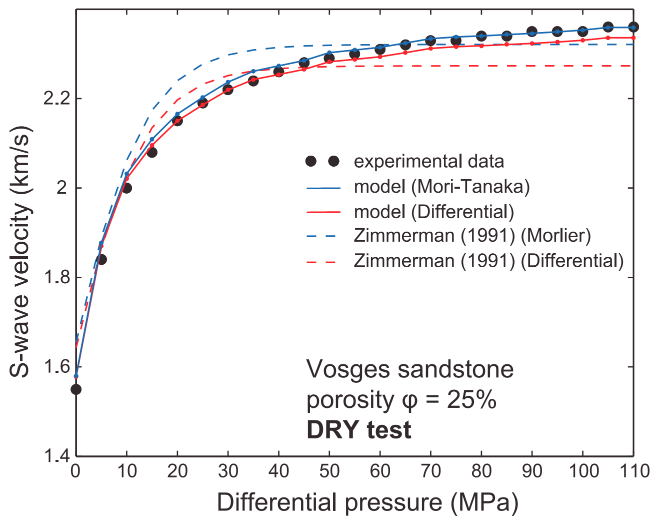

Figure 2. Inversion of V_s, shear seismic velocity, for a dry Vosges sandstone (data after *Fortin et al.* [2007]). The present model is compared to *Zimmerman* [1991] for the Mori-Tanaka and Differential schemes.

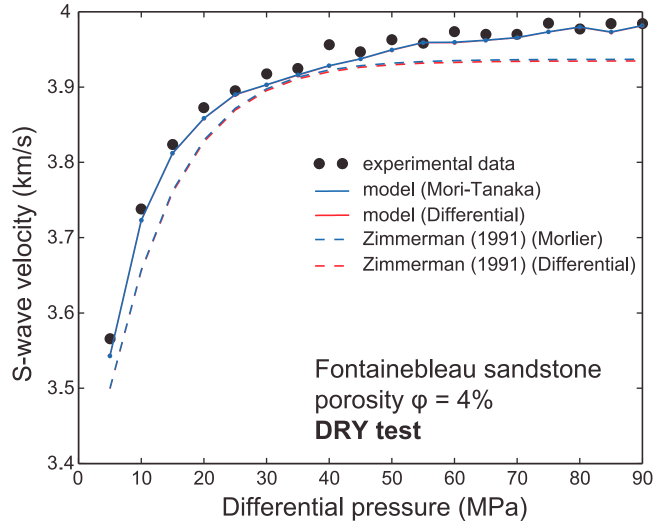

Figure 4. Inversion of V_s, shear seismic velocity, for a dry Fontainebleau sandstone (data after *David* [2012]). The present model is compared to *Zimmerman* [1991] for the Mori-Tanaka and Differential schemes.

(goodness of fit: ($R^2 = 0.971$)); according to the Differential scheme, $\Gamma(p) = 0.458e^{-p/13.6}$ ($R^2 = 0.976$). For the Fontainebleau sandstone, according to the Mori-Tanaka scheme, $\Gamma(p) = 0.226e^{-p/11.8}$ ($R^2 = 0.973$); according to the Differential scheme $\Gamma(p) = 0.192e^{-p/13.1}$ ($R^2 = 0.975$). As explained in section 2.1.4, the resulting aspect ratio distributions functions, which are shown in Figures 5 and 6 and Figures 7 and 8 for the Vosges and Fontainebleau sandstones, respectively, are calculated from equation (25) using the exponential curve fits $\Gamma(p)$. As noted above, for the case of non-closable pores, the Differential scheme infers the presence of a smaller number of cracks that have a higher aspect ratio compared to the Mori-Tanaka scheme; such a result has also been obtained by *Zimmerman* [1991]. This is particularly clear when looking at the crack porosity distribution function, $c(\alpha)$. The aspect ratio distribution function of the cumulative crack porosity, $C(\alpha)$, reaches an asymptotic value, as expected, which gives an estimation of the total crack porosity in the rock. Furthermore, it provides *a posteriori* verification that the contribution of crack porosity to the total porosity is negligible, which was initially assumed (see Figures 6 and 8).

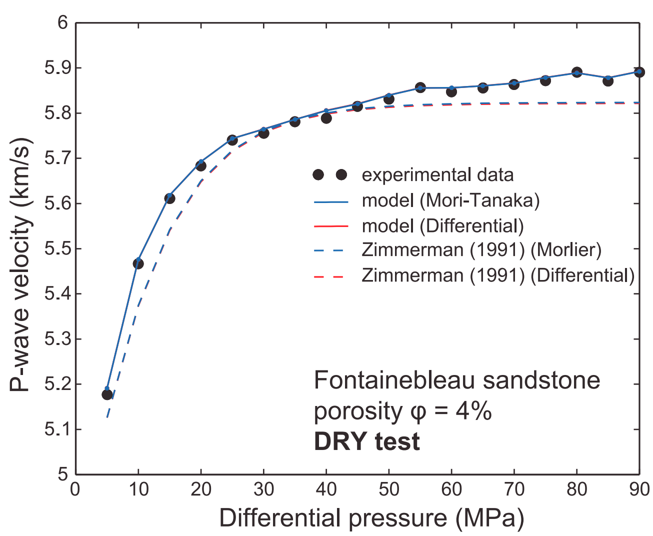

Figure 3. Inversion of V_p, compressional seismic velocity, for a dry Fontainebleau sandstone (data after *David* [2012]). The present model is compared to *Zimmerman* [1991] for the Mori-Tanaka and Differential schemes.

3. Prediction of Saturated Velocities

3.1. Methods for Predicting Saturated Velocities From Dry Velocities

3.1.1. Using the Gassmann Equations

[32] It has been shown above that the pore aspect ratio distribution can be extracted from the pressure dependence of elastic wave velocities on dry rocks. In a rock that is fully saturated with fluid, at a given differential stress the pore structure should be the same as for a dry test (at the same differential stress).

[33] The process of elastic wave propagation is generally assumed to occur under undrained conditions. Gassmann's equations [*Gassmann*, 1951] give the saturated undrained elastic moduli in terms of the porosity of the rock, the compressibilities of the pore fluid and the grains, and the drained elastic moduli of the rock which, according to Gassmann's model, are equivalent to the dry moduli. The

Table 3. Fitting Parameters for the Pressure Dependence of Bulk Compressibility C_{bc}, According to Equation (7)

Sandstone	C^{i}_{bc} (/MPa)	C^{hp}_{bc} (/MPa)	$\hat{p}$ (MPa)	Goodness (R^2)
Vosges	0.212	0.081	7.8	0.981
Fontainebleau	0.046	0.030	9.7	0.966

Table 4. Inversion Results for the High-Pressure Velocities (Zimmerman's Method)

Sandstone	α^{hp} (MT)	Error on (V_p^{hp}, V_s^{hp}) (MT)	α^{hp} (DEM)	Error on (V_p^{hp}, V_s^{hp}) (DEM)
Vosges	0.12[a]	2.2%[c]	0.18[a]	3.8%[c]
Fontainebleau	0.28[b]	1.2%[d]	0.29[b]	1.2%[d]

[a]With K_0 = 39 GPa, G_0 = 24 GPa, see Table 2.
[b]Taking K_0 = 37 GPa, G_0 = 44 GPa, see Table 2.
[c]Compared with measured values for (V_p, V_s) at the highest pressure (110 MPa).
[d]Compared with measured values for (V_p, V_s) at the highest pressure (90 MPa).

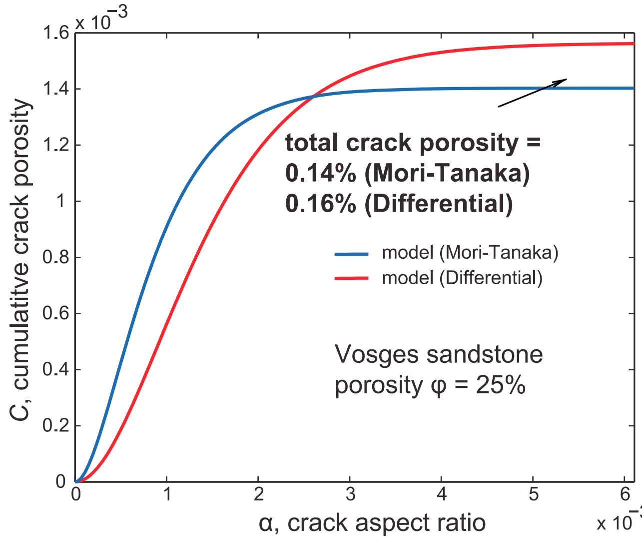

Figure 6. Aspect ratio distribution of the cumulative crack porosity, $C(\alpha)$ (see equation (29)), for a Vosges sandstone (data after *Fortin et al.* [2007]).

expressions for the undrained bulk and shear moduli (K_u, G_u) are [*Brown and Korringa*, 1975]

$$K_u = K_d + \frac{(K_0 - K_d)^2}{(K_0 - K_f)\phi + (K_0 - K_d)}, \tag{30}$$

$$G_u = G_d, \tag{31}$$

where K_f is the bulk modulus of the pore fluid, and (K_d, G_d) are the *dry* bulk and shear moduli. Gassmann's equations have the advantage of predicting saturated velocities without any assumption on the microstructure, using only the dry moduli. However, the Gassmann model assumes local pore fluid equilibrium between the pores, whereas it is very likely that when elastic wave velocities are measured at high-frequencies (~MHz) in fluid-saturated samples, the fluid behaves in the pores as if each pore were isolated from its neighbors with regards to fluid flow. The limiting frequency for local flow between adjacent pores, is [*O'Connell and Budiansky*, 1977; *Palmer and Traviola*, 1981]:

$$f \sim \frac{K_0 \alpha^3}{\eta}, \tag{32}$$

where α is a characteristic aspect ratio of the pores, and η is the viscosity of the pore fluid. For the sandstones considered in this study, ($K_0 \sim 50$ GPa, $\alpha \sim 10^{-3}$), saturated with water ($\eta = 10^{-3}$ Pa.s), this expression yields $f \sim 50$ kHz. The velocities measured in the laboratory were measured at much higher frequencies, implying that it may be more appropriate to treat each pore as being isolated, in which case the effective elastic moduli should be estimated using an effective medium theory, with the inclusion phase being the pore fluid.

3.1.2. Using Effective Medium Theories

[34] According to the Mori-Tanaka scheme, the effective bulk and shear moduli ($\bar{K}, \bar{G}$) of a medium containing fluid-

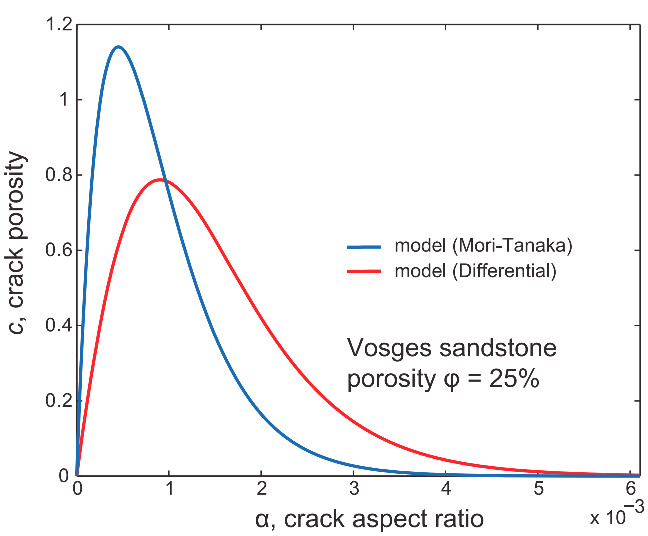

Figure 5. Crack porosity distribution function, $c(\alpha)$ (see equation (28)), for a Vosges sandstone (data after *Fortin et al.* [2007]).

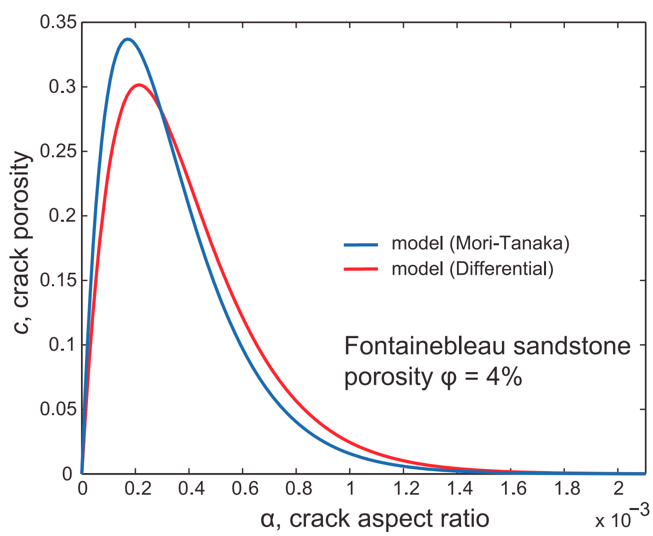

Figure 7. Crack porosity distribution function, $c(\alpha)$ (see equation (28)), for a Fontainebleau sandstone (data after *David* [2012]).

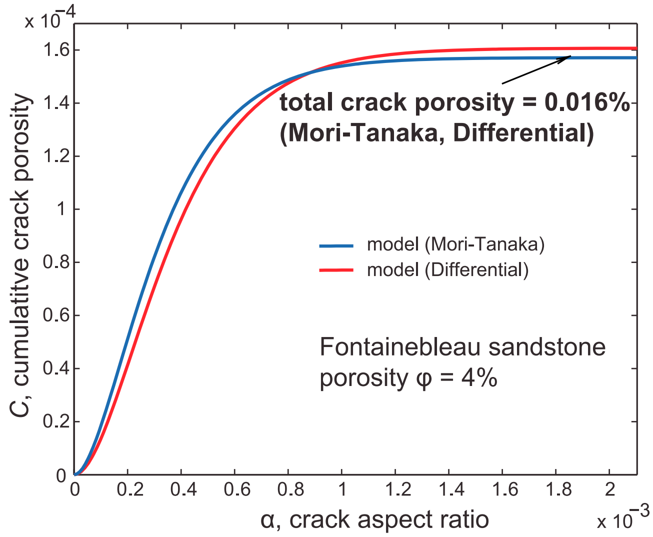

Figure 8. Aspect ratio distribution of the cumulative crack porosity, $C(\alpha)$ (see equation (29)), for a Fontainebleau sandstone (data after *David* [2012]).

saturated pores having an aspect ratio α are given by [*Benveniste*, 1987]

$$\frac{K_0}{\bar{K}} = 1 + \left(\frac{\phi}{1-\phi}\right)\left[\frac{P_u\left(1-\frac{K_f}{K_0}\right)}{1+\left(\frac{\phi}{1-\phi}\right)\frac{K_f}{K_0}P_u}\right], \tag{33}$$

$$\frac{G_0}{\bar{G}} = 1 + \left(\frac{\phi}{1-\phi}\right)Q_u, \tag{34}$$

where (P_u, Q_u) are respectively the normalized *undrained* pore compressibility and shear compliance of the fluid-saturated pore. Exact expressions can be found in *Berryman* [1980] that give P_u and Q_u as functions of α, K_f/K_0, and ν_0.

[35] According to the Differential scheme, for fluid-saturated pores, equations (5)–(6) become [*LeRavalec and Guéguen*, 1996]

$$(1-\phi)\frac{1}{\bar{K}}\frac{d\bar{K}}{d\phi} = -P_u\left(1-\frac{K_f}{\bar{K}}\right), \tag{35}$$

$$(1-\phi)\frac{1}{\bar{G}}\frac{d\bar{G}}{d\phi} = -Q_u, \tag{36}$$

with the initial conditions $\bar{K}(\phi = 0) = K_0$ and $\bar{G}(\phi = 0) = G_0$.

3.1.2.1. High-Pressure Moduli

[36] To predict the effective elastic moduli of the fluid-saturated rock as functions of pressure, the first step is to calculate the high-pressure elastic moduli of the "matrix" that is formed by the minerals plus the saturated non-closable pores. These values are denoted by $(\bar{K}^{hp,mt}, \bar{G}^{hp,mt})$ and $(\bar{K}^{hp,dem}, \bar{G}^{hp,dem})$ for the Mori-Tanaka and the Differential schemes, respectively. As the "high-pressure" pore structure is assumed to be the same as for the dry test, $(\bar{K}^{hp,mt}, \bar{G}^{hp,mt})$ and $(\bar{K}^{hp,dem}, \bar{G}^{hp,dem})$ are simply obtained by using α^{hp}, the aspect ratio of the non-closable pores previously inverted from dry data, ϕ, the total porosity (which is still assumed to be accounted for by the non-closable pores) and (K_0, G_0), elastic moduli of the minerals, as input parameters in equations (33)–(34) and (35)–(36), respectively.

3.1.2.2. Effect of Cracks

[37] The second step, which now considers the effect of cracks, is not trivial. For saturated thin-cracks, the expressions giving the effective moduli depend on the crack density, but also on the aspect ratio of the cracks [*Fortin et al.*, 2007]. Hence, at each pressure, the individual crack contributions to the compliance, due to the open cracks, must be summed up. However, in contrast to the dry case (see section 2.1.2), it will not be possible to directly use the total crack density Γ to quantify the effective moduli.

[38] Consider a pressure stage p. According to section 2.1.3, the open cracks in the rock are the cracks having an initial aspect ratio α^i greater than $\alpha^\star(p)$. According to equation (20), their aspect ratio at pressure p has now become $\alpha(p) = \alpha^i - \alpha^\star(p)$, where the calculation of $\alpha^\star(p)$ from equation (21) depends on the effective medium theory considered. From this point onwards, the model will be developed separately for the two different effective medium theories.

[39] *Mori-Tanaka scheme.* According to the Mori-Tanaka scheme, the contribution of cracks is calculated as if they were non-interacting. Hence, the crack closure equation (21) becomes

$$\alpha^\star = \int_0^p \frac{4\left[1-\left(\nu^{hp,mt}\right)^2\right]}{3\pi K^{hp,mt}\left(1-2\nu^{hp,mt}\right)}dp' = \frac{4\left[1-\left(\nu^{hp,mt}\right)^2\right]}{3\pi K^{hp,mt}\left(1-2\nu^{hp,mt}\right)}p, \tag{37}$$

where the elastic moduli of the "high-pressure" host material $(K^{hp,mt}, \nu^{hp,mt})$ are taken to be equal to the *dry* moduli.

[40] For saturated cracks having an aspect ratio α, the general expressions for the Mori-Tanaka scheme (33)–(34) giving the effective moduli reduce to the no-interaction approximation:

$$\frac{K_0}{\bar{K}} = 1 + \phi\left(1-\frac{K_f}{K_0}\right)P_u(\alpha, K_f/K_0, \nu_0), \tag{38}$$

$$\frac{G_0}{\bar{G}} = 1 + \phi Q_u(\alpha, K_f/K_0, \nu_0), \tag{39}$$

where the arguments of the undrained pore compliances (P_u, Q_u) are now explicitly written. The initial porosity of cracks having an initial aspect ratio between α^i and $\alpha^i + d\alpha^i$ is, by definition, $c(\alpha^i)d\alpha^i$. At pressure p, according to the previous considerations on the change of crack geometry during closure (see section 2.1.3), and to the crack closure model (equation (20)), the porosity of such cracks is now $c(\alpha^i)d\alpha^i(1 - \alpha^\star/\alpha^i)$. Hence, equations (38)–(39) are used to add the individual crack contributions, for all open cracks $(\alpha^i > \alpha^\star)$. Remembering that the effective moduli of the host

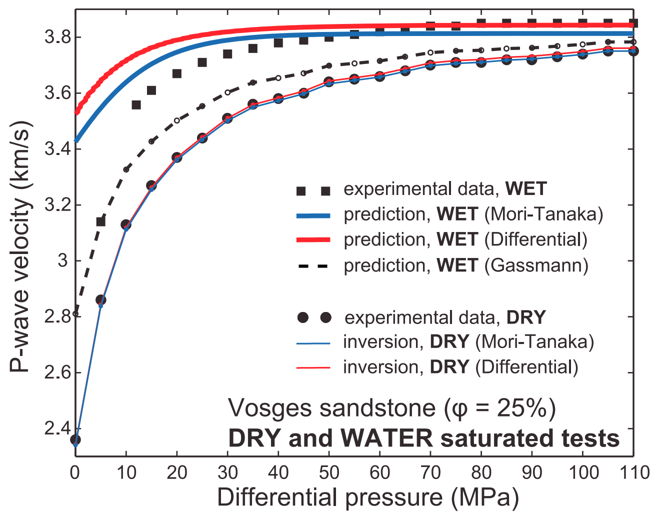

Figure 9. Predictions for the compressional seismic velocity for a water-saturated Vosges sandstone, according to Gassmann's equation (using the dry velocity data, *cf.* section 3.1.1), or alternatively using the aspect ratio distributions (inverted from dry data) as input in effective medium schemes (Mori-Tanaka, Differential, *cf.* section 3.1.2). The inverted dry velocities (see Figure 1) are also shown (data after *Fortin et al.* [2007]).

material are $(\bar{K}^{\mathrm{mt,hp}}, \bar{G}^{\mathrm{mt,hp}})$, the saturated effective moduli $(\bar{K}, \bar{G})$ are now given by

$$\frac{\bar{K}^{\mathrm{mt,hp}}}{\bar{K}(p)} = 1 + \int_{\alpha^{\mathrm{i}} > \alpha^\star(p)} \left[c(\alpha^{\mathrm{i}}) \left(1 - \frac{\alpha^\star(p)}{\alpha^{\mathrm{i}}}\right) \left(1 - \frac{K_{\mathrm{f}}}{\bar{K}^{\mathrm{mt,hp}}}\right) \times P_{\mathrm{u}}\left(\alpha^{\mathrm{i}} - \alpha^\star(p), K_{\mathrm{f}}/\bar{K}^{\mathrm{mt,hp}}, \bar{\nu}^{\mathrm{mt,hp}}\right)\right] \mathrm{d}\alpha^{\mathrm{i}}, \tag{40}$$

$$\frac{\bar{G}^{\mathrm{mt,hp}}}{\bar{G}(p)} = 1 + \int_{\alpha^{\mathrm{i}} > \alpha^\star(p)} \left[c(\alpha^{\mathrm{i}}) \left(1 - \frac{\alpha^\star(p)}{\alpha^{\mathrm{i}}}\right) \times Q_{\mathrm{u}}\left(\alpha^{\mathrm{i}} - \alpha^\star(p), K_{\mathrm{f}}/\bar{K}^{\mathrm{mt,hp}}, \bar{\nu}^{\mathrm{mt,hp}}\right)\right] \mathrm{d}\alpha^{\mathrm{i}}. \tag{41}$$

Knowing the crack porosity distribution function, $c(\alpha)$, the integrals can be calculated at each pressure by numerical integration.

[41] *Differential scheme.* For the Differential scheme, the crack closure equation (21) becomes

$$\alpha^\star = \int_0^p \frac{4\left[1 - \nu(p')^2\right]}{3\pi K(p')[1 - 2\nu(p')]} \mathrm{d}p', \tag{42}$$

where, according to the Differential scheme, the elastic parameters (K, ν) of the (dry) porous rock depend on pressure. They can be calculated combining the exponential curve fit $\Gamma(p)$ (equation (27)) with the effective medium model (equations (13)–(14)).

[42] For the Differential scheme, the effective moduli at each pressure cannot simply be expressed in closed-form expressions as in equations (40)–(41), but can be calculated by iteration, using the following thought experiment. First, cracks are introduced into the high pressure host material, when all cracks are closed, along a fictitious unloading path. If p is decreased by a small increment dp, the cracks that are open are the cracks having initial aspect ratios $\alpha^{\mathrm{i}} > \alpha^\star(p - \mathrm{d}p)$, where $\alpha^\star(p - \mathrm{d}p)$ is calculated from equation (42). Since dp is small, it can be assumed the aspect ratio of the small fraction of open cracks is constant. The porosity of such cracks is, according to previous considerations, $c(\alpha^{\mathrm{i}})\mathrm{d}\alpha^{\mathrm{i}}(1 - \alpha^\star/\alpha^{\mathrm{i}})$. Hence, the effective moduli can be calculated by solving the differential equations (35)–(36), where the moduli of the host material are the "high-pressure" moduli of the rock with no cracks. This procedure can be repeated by continually decreasing the pressure by small increments; at each step, the differential equations are solved, introducing the small number of cracks that re-open between the two pressure stages, into the host material that contains the influence of the other cracks that were already open at higher pressures. This method introduces cracks by small increments in an order that seems to be natural; moreover, it has been shown that the order in which pores are added in the differential equations has a very small influence on the overall effective moduli [*LeRavalec and Guéguen*, 1996].

3.2. Application of Model to Experimental Data on Sandstones

[43] In section 2.2 the aspect ratio distributions for the Vosges and Fontainebleau sandstones were obtained by matching the dry data. For both such experiments, P and S-wave velocities were also measured for water-saturated tests, using a constant pore pressure p_{p} = 10 MPa for the Vosges sandstone, and p_{p} = 5 MPa for the Fontainebleau sandstone.

[44] The saturated velocities can first be estimated using Gassmann's relations (equations (30)–(31)). This process is straightforward and does not depend on the inversion of dry data: the bulk and shear moduli of the minerals are already known (see section 2.2), the total porosity is measured, the bulk modulus of water, at pressure of 10 MPa, is K_{f} = 2.24 GPa (for the Vosges sandstone) and, at pressure of 5 MPa, is K_{f} = 2.20 GPa (for the Fontainebleau sandstone) [*Coyner*, 1984], and the drained moduli, which are identified with the dry moduli, are directly measured by seismic velocities.

[45] The seismic velocities at high-frequency can also be estimated using the pore aspect ratio distribution previously inverted from dry data (see section 2.2) as input in the Mori-Tanaka and Differential schemes, using the method presented in section 3.1. Note that the use of either the Gassmann equations or an effective medium theory yields estimated values of the saturated moduli, which are in turn converted into saturated velocities by using the appropriate saturated rock density, $\bar{\rho}$ $(\bar{\rho} = \rho + \phi\rho_{\mathrm{f}}$ where, for water, ρ_{f} = 1000 kg/m^3).

[46] The first conclusion that can be reached from the results obtained for Vosges and Fontainebleau sandstones (Figures 9–13 and 14–18, respectively) is that the Gassmann model always predicts a much more compliant behavior than is measured from ultrasonic velocities. The saturated velocities are *underpredicted* by Gassmann's equations by a large amount that exceeds the uncertainty of the measurements (which, for the traveltime method, are considered to be less than 3% [*Bourbié et al.*, 1986; *Fortin et al.*, 2007]). This has

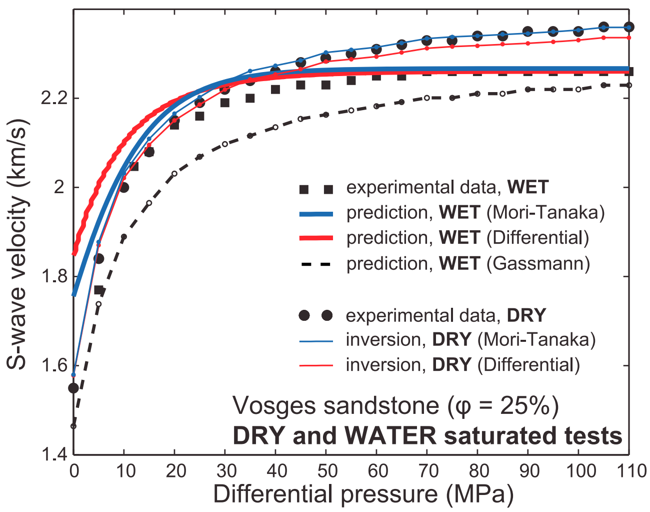

Figure 10. Predictions for the shear seismic velocity for a water-saturated Vosges sandstone, according to Gassmann's equation (using the dry velocity data, *cf.* section 3.1.1), or alternatively using the aspect ratio distributions (inverted from dry data) as input in effective medium schemes (Mori-Tanaka, Differential, *cf.* section 3.1.2). The inverted dry velocities (see Figure 2) are also shown (data after *Fortin et al.* [2007]).

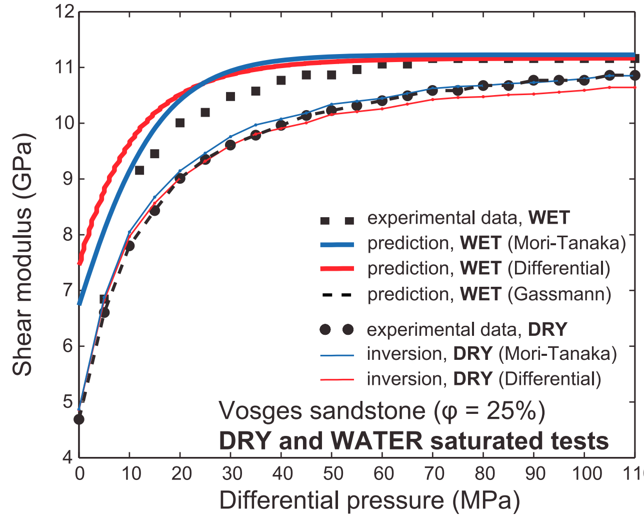

Figure 12. Predictions for the effective shear modulus for a water-saturated Vosges sandstone, according to Gassmann's equation (using the dry velocity data, *cf.* section 3.1.1), or alternatively using the aspect ratio distributions (inverted from dry data) as input in effective medium schemes (Mori-Tanaka, Differential, *cf.* section 3.1.2). The inverted dry moduli are also shown (data after *Fortin et al.* [2007]).

been observed for many more sets of experimental data on sandstones, such as those obtained by *King* [1966], *Coyner* [1984] (see *David* [2012]), or *King and Marsden* [2002], who have also noted that Gassmann's predictions become reasonably accurate at high-pressures, which is indeed observed in the present results. Note that similar such conclusions were also reported for other type of porous rocks, such as carbonates [*Agersborg et al.*, 2008] or basalt [*Adelinet et al.*, 2010]. In contrast, effective medium theories do a good job in predicting the saturated elastic behavior at all pressures, especially for the Fontainebleau sandstone. In particular, the predictions for Poisson's ratio as a function of pressure are also excellent. Another remarkable result is that the quality of the fits are only very weakly dependent on the choice of the effective medium theory.

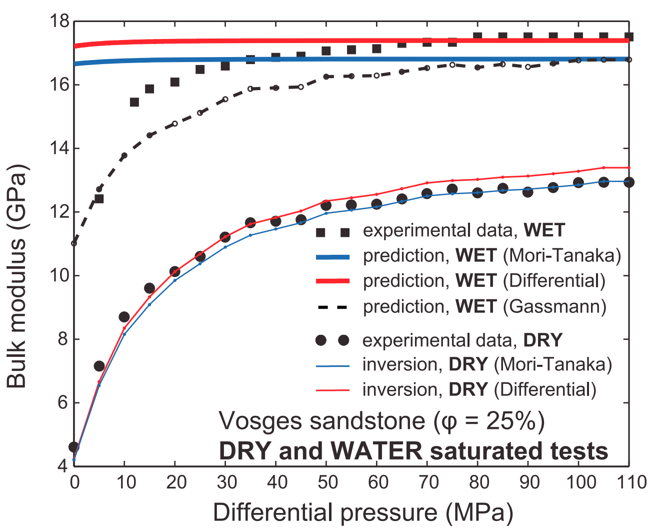

Figure 11. Predictions for the effective bulk modulus for a water-saturated Vosges sandstone, according to Gassmann's equation (using the dry velocity data, *cf.* section 3.1.1), or alternatively using the aspect ratio distributions (inverted from dry data) as input in effective medium schemes (Mori-Tanaka, Differential, *cf.* section 3.1.2). The inverted dry moduli are also shown (data after *Fortin et al.* [2007]).

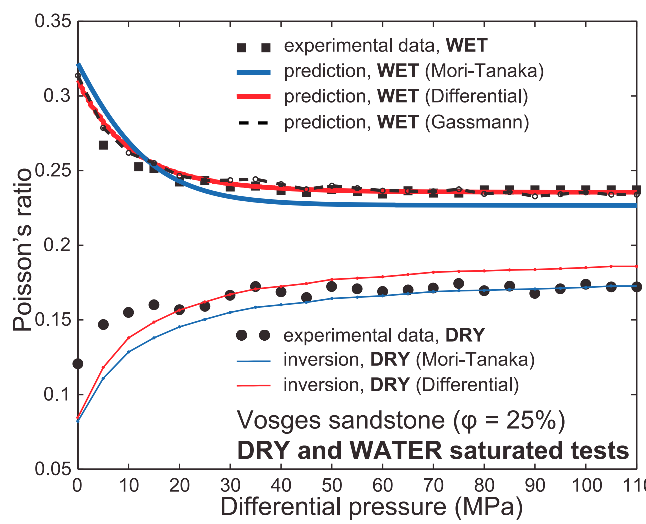

Figure 13. Predictions for the effective Poisson's ratio for a water-saturated Vosges sandstone, according to Gassmann's equation (using the dry velocity data, *cf.* section 3.1.1), or alternatively using the aspect ratio distributions (inverted from dry data) as input in effective medium schemes (Mori-Tanaka, Differential, *cf.* section 3.1.2). The inverted dry Poisson's ratios are also shown (data after *Fortin et al.* [2007]).

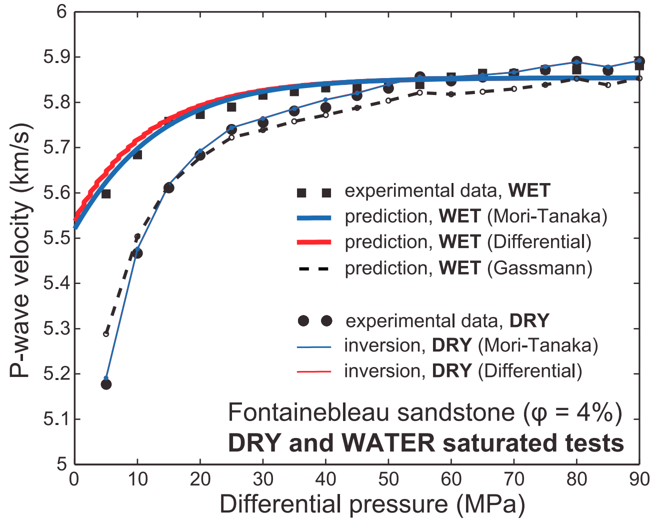

Figure 14. Predictions for the compressional seismic velocity for a water-saturated Fontainebleau sandstone, according to Gassmann's equation (using the dry velocity data, *cf.* section 3.1.1), or alternatively using the aspect ratio distributions (inverted from dry data) as input in effective medium schemes (Mori-Tanaka, Differential, *cf.* section 3.1.2). The inverted dry velocities (see Figure 3) are also shown (data after *David* [2012]).

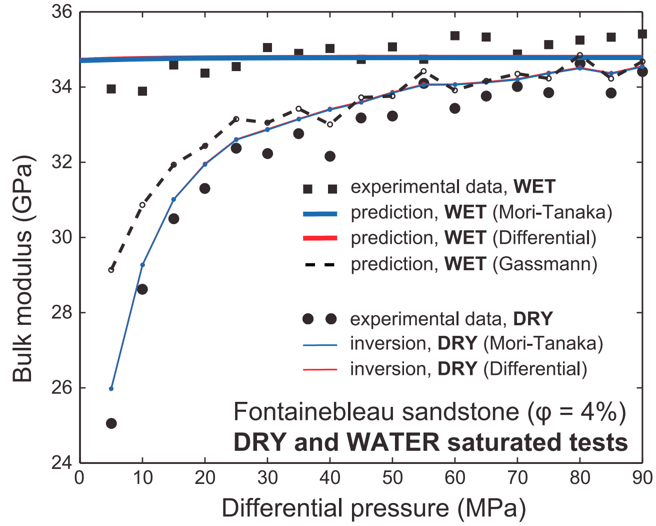

Figure 16. Predictions for the effective bulk modulus for a water-saturated Fontainebleau sandstone, according to Gassmann's equation (using the dry velocity data, *cf.* section 3.1.1), or alternatively using the aspect ratio distributions (inverted from dry data) as input in effective medium schemes (Mori-Tanaka, Differential, *cf.* section 3.1.2). The inverted dry moduli are also shown (data after *David* [2012]).

[47] Effective medium models often assume that the effective bulk modulus of a solid with saturated thin cracks is equal to solid's bulk modulus [*Budiansky and O'Connell*, 1976; *Henyey and Pomphrey*, 1982]. For the sandstones considered here, this implies that the effect of the fluid on saturated bulk modulus only comes from the presence of the stiff, "equant" pores, and that this effect should not depend on pressure. Although this assumption for predicting the elastic behavior of saturated cracks was not used in the present model, the predictions indeed show a very weak pressure dependence of saturated bulk modulus, with reasonably good

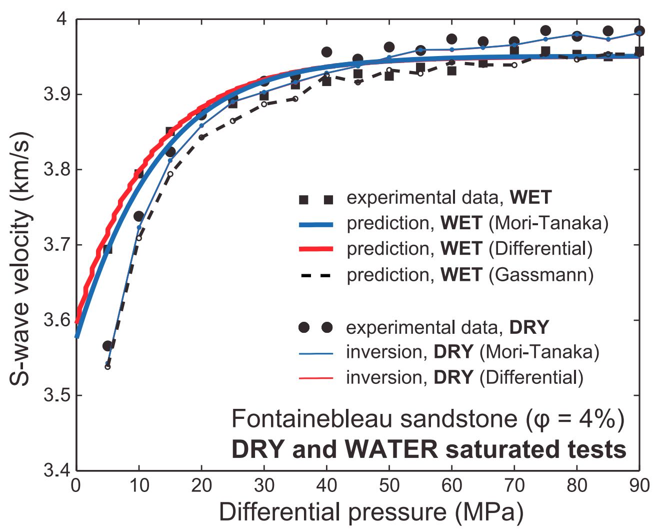

Figure 15. Predictions for the shear seismic velocity for a water-saturated Fontainebleau sandstone, according to Gassmann's equation (using the dry velocity data, *cf.* section 3.1.1), or alternatively using the aspect ratio distributions (inverted from dry data) as input in effective medium schemes (Mori-Tanaka, Differential, *cf.* section 3.1.2). The inverted dry velocities (see Figure 4) are also shown (data after *David* [2012]).

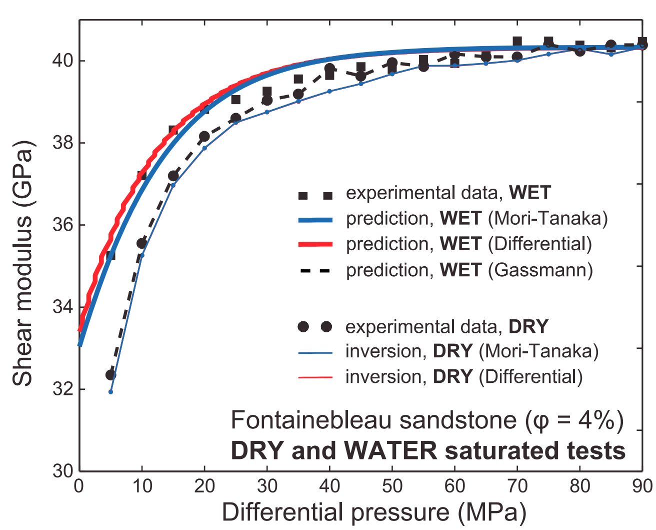

Figure 17. Predictions for the effective shear modulus for a water-saturated Fontainebleau sandstone, according to Gassmann's equation (using the dry velocity data, *cf.* section 3.1.1), or alternatively using the aspect ratio distributions (inverted from dry data) as input in effective medium schemes (Mori-Tanaka, Differential, *cf.* section 3.1.2). The inverted dry moduli are also shown (data after *David* [2012]).

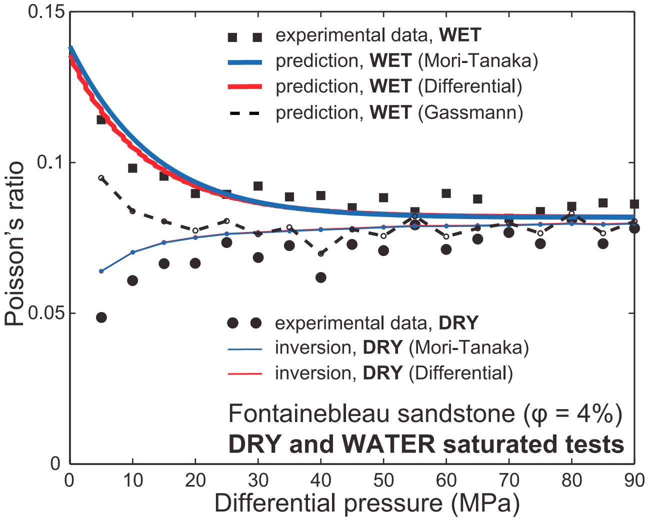

Figure 18. Predictions for the effective Poisson's ratio for a water-saturated Fontainebleau sandstone, according to Gassmann's equation (using the dry velocity data, *cf.* section 3.1.1), or alternatively using the aspect ratio distributions (inverted from dry data) as input in effective medium schemes (Mori-Tanaka, Differential, *cf.* section 3.1.2). The inverted dry Poisson's ratios are also shown (data after *David* [2012]).

agreement with the data. In contrast, Gassmann's predictions for saturated bulk modulus fail at low pressures, but interestingly, as the pressure increases and cracks successively close up, they become very close to the predictions of effective medium theories. This observation is in agreement with theoretical predictions: for a solid containing only *one* family of pores (each with the same aspect ratio), having random orientations, the saturated effective bulk modulus calculated using the Mori-Tanaka scheme is precisely consistent with the predictions of the Gassmann equations [*Suvorov and Selvadurai*, 2011]; this is not exactly true for the Differential scheme, however [*Berryman et al.*, 2002].

[48] The case of the shear modulus is even more interesting. It has long been observed on some sandstones that the saturated shear wave velocity can be higher than the dry shear velocity [*King*, 1966; *Coyner*, 1984]. This happens especially at low pressures, and can then be attributed to the presence of open cracks, as in general there is a crossover at intermediate pressures (see Figures 12 and, above all, Figure 17) where the saturated shear velocity again becomes lower than the dry shear velocity. The Gassmann model assumes that the pore fluid has no effect on the shear modulus (see equation (31)); since saturated rocks are always denser than dry rocks, the density effect causes the saturated shear velocity predicted by the Gassmann model to be always lower than the dry shear velocity. It can clearly be seen that the results predicted by the Gassmann model for the saturated shear velocity are in contradiction with the experimental data (see Figures 12 and 17). In contrast, the new spheroidal pore model is able to predict the stiffening effect of saturated cracks in shear, at low pressures, which now needs to be explained. For an anisotropic stress field such as a shear wave traveling through the rock, pore pressure changes are very sensitive to pore orientation [*Shafiro and Kachanov*, 1997]. For cracks having particular orientations, under shear, the *resolved traction* on a crack surface can be *compressive.* As it is assumed in effective medium modeling that each crack is individually undrained, for a certain number of cracks, the pore fluid will offer a resistance (the fluid compressibility is implicitly contained in the expressions for the undrained pore shear compliance Q_u, see section 3.1.2). This results in a higher effective shear modulus for a fluid-saturated rock than for a dry rock, providing that the frequency of the wave (and, then, of stress perturbations) is sufficiently high to prevent any fluid from leaving the pores. Moreover, *Shafiro and Kachanov* [1997] have also shown that, during the passing of a wave, pore pressure changes highly depend on the pore aspect ratio: a shear wave will induce pore pressure changes for thin cracks (small α), but this effect vanishes as α increases and the pores become spherical. This explains the important difference between the Gassmann model and the effective medium theories in predicting saturated shear modulus at low pressures, which becomes very small at high pressures, when the rock body is only left with nearly spherical pores (see, in particular, the case of Fontainebleau sandstone (Figure 17) which has the highest values of α^{hp}, see Table 2).

[49] Additional evidence that the elastic behavior of fluid-saturated rocks during ultrasonic measurements is better predicted by effective medium theories than by the Gassmann equations can be obtained by estimating the critical frequency for fluid flow between pores (equation (32)) for the Vosges and Fontainebleau sandstones, whose measured permeabilities are 20 mD [*Fortin et al.*, 2007] and 0.1 mD *David* [2012], respectively. Using the inferred aspect ratios of 1.0×10^{-3} and 0.2×10^{-3} (see Figures 5 and 7, respectively), a viscosity $\eta = 10^{-3}$ (for water), and the values of K_0 given in Table 2, one obtains $f = 40$ kHz for the Vosges sandstone and $f = 300$ Hz for the Fontainebleau sandstone. It is therefore reasonable to assume that, during ultrasonic measurements ($f \sim 1$ MHz), the fluid is trapped in the individual pores. This might not be true for wave velocities measurements methods that are used at intermediate to low frequencies, such as in field logging, or seismology. Effective medium theories, however, will always predict an *upper bound* for the elastic moduli.

[50] This pore structure model has been tested against many other sets of experimental data on sandstones [*David*, 2012]. The model is able to invert most sets of dry data, using an exponential distribution of crack aspect ratios, and only one aspect ratio for the non-closable pores. Nevertheless, the predictions for ultrasonic saturated velocities obtained using an effective medium theory, although always better than those obtained using the Gassmann equations, are not always sufficiently accurate. From a theoretical point of view, the intrinsic limits of using a spheroidal model for pores in sandstones seem to be reached. More precisely, it has been observed that the lack of accuracy in the predictions is always mostly due to a misfit in the saturated bulk modulus $\bar{K}$: on the one hand, the use of one aspect ratio is sometimes inaccurate in predicting the high-pressure data; on the other hand, as noted before, the lack of pressure dependence of $\bar{K}$ is in disagreement with the data. From an

experimental point of view, it is well known that ultrasonic measurements are much more accurate in predicting *relative* evolution of velocities with pressure than *absolute* values [*Fortin et al.*, 2007]. The model is also very sensitive to parameters such as fluid compressibility and, above all, the bulk and shear moduli of the minerals (K_0, G_0), which are often not very well constrained by the experiments. For instance, the values given in *Coyner* [1984] for K_0 measured by unjacketed tests sometimes lie outside of the Voigt-Reuss bounds calculated from the mineralogical composition.

4. Conclusions

[51] Zimmerman's method for inverting dry velocities has been extended to obtain the complete distribution of crack aspect ratios, as well as the average aspect ratio of the non-closable pores, by fitting both compressional and shear wave velocities. The new method, which can be used in conjunction with any effective medium theory, is able to invert successfully many sets of experimental data on sandstones. It remains simple, as the inversion is performed on dry data only, therefore avoiding the need to take into account the pore fluid, which masks the effect of pore geometry. The resulting crack aspect ratio distribution is exponential, and the inversion of high-pressure velocities (when the rock is crack-free) shows that the non-closable pores are well represented by one family of oblate spheroids, which show significant deviations from sphericity. Models assuming that non-closable pores are spherical are therefore not realistic for most sandstones.

[52] The saturated velocities can be predicted by the Gassmann equations, or by using effective medium theories. The Gassmann predictions, which are straightforward and can be done directly from dry data without any assumption on the microstructure, underestimate the saturated high-frequency velocities by a large amount. Hence, a method has also been developed to predict the saturated velocities using effective medium theories (which assume that fluid is totally trapped in each pore), making use of the pore aspect ratio distribution that has been obtained from the dry data. The results show that effective medium theories are able to predict well the saturated velocities for many sets of experimental data on sandstones. The conclusion that saturated velocities are better predicted by effective medium theories than by using the Gassmann equations might not hold at lower frequencies, such as in the field. This raises the need for more experimental data on elastic wave velocities at intermediate to low frequencies, to be able to better understand the influence of fluid flow within the pore space on the overall elastic velocities.

[53] Although idealized as regards to real pore shapes in sandstones, the spheroidal model for pores seems to be capable of explaining the stress dependence of dynamic (present work) as well as static [*Walsh*, 1965] elastic properties of sandstones. Moreover, the results are only weakly dependent of the choice of the effective medium theory (Mori-Tanaka or Differential scheme), which leaves the contentious debate of which effective medium theory best accounts for interactions between pores beyond the scope of this present work. It is likely that this work has taken the use of the simple spheroidal pore model as far as possible, as it has been found that this model is not able to predict saturated velocities with sufficient accuracy for some sandstones [*David*, 2012]. Moreover, the non-linear elastic behavior during hydrostatic compression was accounted for by assuming that a porous rock contains a *distribution* of aspect ratios: such an assumption is required if the spheroidal model for pores is used, but not necessarily for other irregular pores shapes [*Mavko and Nur*, 1978]. In particular, some papers have considered non-elliptical two-dimensional pores such as hypotrochoidal tubes [*Mavko*, 1980], quasi-polygons [*Kachanov et al.*, 1994; *Jasiuk et al.*, 1994], pores having *n*-fold axis of symmetry [*Ekneligoda and Zimmerman*, 2006, 2008], or arbitrary irregular shapes [*Tsukrov and Novak*, 2004], as the basis of their calculations.

[54] **Acknowledgments.** We thank Jérome Fortin (ENS Paris, France) for providing experimental data set tables obtained on Vosges sandstone [*Fortin et al.*, 2007].

References

Adelinet, M., J. Fortin, Y. Guéguen, A. Schubnel, and L. Geoffroy (2010), Frequency and fluid effects on elastic properties of basalt: Experimental investigations, *Geophys. Res. Lett.*, *37*, L02303, doi:10.1029/2009GL041660.

Adelinet, M., C. Dorbath, M. Le Ravalec, J. Fortin, and Y. Guéguen (2011), Deriving microstructure and fluid state within the Icelandic crust from the inversion of tomography data, *Geophys. Res. Lett.*, *38*, L03305, doi:10.1029/2010GL046304.

Agersborg, R., T. A. Johansen, M. Jakobsen, J. Sothcott, and A. Best (2008), Effects of fluids and dual-pore systems on pressure-dependent velocities and attenuations in carbonates, *Geophysics*, *73*, N35–N47.

Benveniste, Y. (1987), A new approach to the application of Mori-Tanaka's theory in composite materials, *Mech. Mater.*, *6*, 147–157.

Berryman, J. G. (1980), Long-wavelength propagation in composite elastic media II. Ellipsoidal inclusions, *J. Acoust. Soc. Am.*, *68*, 1820–1831.

Berryman, J. G., S. R. Pride, and H. F. Wang. (2002), A differential scheme for elastic properties of rocks with dry or saturated cracks, *Geophys. J. Int.*, *151*, 597–611.

Bourbié, T., O. Coussy, and B. Zinszner (1986), *Acoustics of Porous Media*, Ed. Technip, Paris.

Brown, R. J. S., and J. Korringa (1975), On the dependence of elastic properties of a porous rock on the compressibility of the pore fluid, *Geophysics*, *40*, 608–616.

Budiansky, B., and R. J. O'Connell (1976), Elastic moduli of a cracked solid, *Int. J. Solids Struct.*, *12*, 81–97.

Cheng, C. H., and M. N. Toksöz (1979), Inversion of seismic velocities for the pore aspect ratio spectrum of a rock, *J. Geophys. Res.*, *84*, 7533–7543.

Coyner, K. B. (1984), Effect of stress, pore pressure, and pore fluids on bulk strain, velocity, and permeability of rocks, PhD thesis, Mass. Inst. of Technol., Cambridge.

David, E. C. (2012), The effect of stress, pore fluid and pore structure on elastic wave velocities in sandstones, PhD thesis, Imperial College London, London.

David, E. C., and R. W. Zimmerman (2011a), Compressibility and shear compliance of spheroidal pores: exact derivation via the Eshelby tensor, and asymptotic expressions in limiting cases, *Int. J. Solids Struct.*, *48*, 680–688.

David, E. C., and R. W. Zimmerman (2011b), Elastic moduli of solids containing spheroidal pores, *Int. J. Eng. Sci. 49*, 544–560.

Ekneligoda, T. C., and R. W. Zimmerman (2006), Compressibility of two-dimensional pores having *n*-fold axes of symmetry, *Proc. R. Soc. London A*, *462*, 1933–1947.

Ekneligoda, T. C., and R. W. Zimmerman (2008), Shear compliance of two-dimensional pores possessing *N*-fold axis of rotational symmetry, *Proc. R. Soc. London A*, *464*, 759–775.

Eshelby, J. D. (1957), The determination of the elastic field of an ellipsoidal inclusion, and related problems, *Proc. R. Soc. London A*, *241*, 376–396.

Ferrari, M. (1994), Composite homogenization via the equivalent poly-inclusion approach, *Composites Eng.*, *4*, 37–45.

Fortin, J., Y. Guéguen, and A. Schubnel (2007), Effects of pore collapse and grain crushing on ultrasonic velocities and V_p/V_s, *J. Geophys. Res.*, *112*, B08207, doi:10.1029/2005JB004005.

Gassmann, F. (1951), On the elasticity of porous media, *Vierteljahrsschr. Naturforsch. Ges. Zurich*, *96*, 1–23.

Henyey, F. S., and N. Pomphrey (1982), Self-consistent elastic moduli of a cracked solid, *Geophys. Res. Lett.*, *9*, 903–906.

Jasiuk, I., J. Chen, and M. F. Thorpe (1994), Elastic moduli of two dimensional materials with polygonal and elliptical holes, *Appl. Mech. Rev.*, *47*, 18–21.
Kachanov, M., I. Tsukrov, and B. Shafiro (1994), Effective moduli of solids with cavities of various shapes, *Appl. Mech. Rev.*, *47*, 152–174.
King, M. S. (1966), Wave velocities in rocks as a function of changes in overburden pressure and pore fluid saturants, *Geophysics*, *31*, 50–73.
King, M. S. (2005), Rock-physics developments in seismic exploration: A personal 50-year perspective, *Geophysics*, *70*, 3ND–8ND.
King, M. S., and J. R. Marsden (2002), Velocity dispersion between ultrasonic and seismic frequencies in brine-saturated reservoir sandstones, *Geophysics*, *67*, 254–258.
Kuster, G. T., and M. N. Toksöz (1974), Velocity and attenuation of seismic waves in two-phase media: Part I. Theoretical formulations, *Geophysics*, *39*, 587–606.
LeRavalec, M., and Y. Guéguen (1996), High- and low-frequency elastic moduli for a saturated porous/cracked rock—Differential self-consistent and poroelastic theories, *Geophysics*, *61*, 1080–1094.
Liu, H. H., J. Rutqvist, and J. G. Berryman (2009), On the relationship between stress and elastic strain for porous and fractured rock, *Int. J. Rock Mech. Min. Sci.*, *46*, 289–296.
MacBeth, C. (2004), A classification for the pressure-sensitivity properties of a sandstone rock frame, *Geophysics*, *69*, 497–510.
Mavko, G. (1980), Velocity and attenuation in partially molten rocks, *J. Geophys. Res.*, *85*, 5173–5189.
Mavko, G., and A. Nur (1978), The effect of nonelliptical cracks on the compressibility of rocks, *J. Geophys. Res.*, *83*, 4459–4468.
Mavko, G., T. Mukerji, and J. Dvorkin (2009), *The Rock Physics Handbook*, Cambridge Univ. Press, Cambridge, U. K.
McLaughlin, R. (1977), A study of the differential scheme for composites materials, *Int. J. Eng. Sci.*, *15*, 237–244.
Mori, T., and K. Tanaka (1973), Average stress in matric and average elastic energy of materials with misfitting inclusions, *Acta Mater.*, *21*, 571–574.
Morlier, P. (1971), Description of the state of rock fracturization through simple non-destructive tests, *Rock Mech.*, *3*, 125–138.
Norris, A. N. (1985), A differential scheme for the effective moduli of composites, *Mech. Mater.*, *4*, 1–16.
O'Connell, R. J., and B. Budiansky (1977), Viscoelastic properties of fluid-saturated cracked solids, *J. Geophys. Res.*, *82*, 5719–5735.
Palmer, I. D., and M. L. Traviola (1981), Attenuation by squirt flow in undersaturated gas sands, *Geophysics*, *45*, 1780–1792.
Salganik, R. L. (1973), Mechanics of bodies with many cracks, *Mech. Solids*, *8*, 135–143.
Shafiro, B., and M. Kachanov (1997), Materials with fluid-filled pores of various shapes: effective elastic properties and fluid pressure polarization, *Int. J. Solids Struct.*, *34*, 3517–3540.
Shapiro, S. A. (2003), Elastic piezosensitivity of porous and fractured rocks, *Geophysics*, *68*, 482–486.
Suvorov, A. P., and A. P. S. Selvadurai (2011), Effective medium methods and a computational approach for estimating geomaterial properties of porous materials with randomly oriented ellipsoidal pores, *Comput. Geotech.*, *38*, 721–730.
Tsukrov, I., and J. Novak (2004), Effective elastic properties of solids with two-dimensional inclusions of irregular shapes, *Int. J. Solids Struct.*, *41*, 6905–6924.
Walsh, J. B. (1965), The effect of cracks on the compressibility of rocks, *J. Geophys. Res.*, *70*, 381–389.
Zimmerman, R. W. (1984), Elastic moduli of a solid with spherical pores: New self-consistent method, *Int. J. Rock Mech. Min. Sci.*, *21*, 339–343.
Zimmerman, R. W. (1991), *Compressibility of Sandstones*, Elsevier, Amsterdam.